

# Snow Avalanches

C. Ancey

*École Polytechnique Fédérale de Lausanne, Ecublens, 1015 Lausanne, Switzerland*

## 1 Introduction

Over the last century, recreational activities, transportation, and constructions in high-altitude areas (ski resorts, dams) have shown a rapid growth in many mountain ranges in Europe and North America. In these areas, snow avalanches are a major threat, causing damage and death. A typical example in recent years is provided by the 1999 winter, where several snow storms hit the Alps, producing huge avalanches, which reached the valley bottoms and killed 62 people inhabitants. The growth in winter sports has also led to a significant increase in avalanche deaths over the last few decades, with some 200 skiers or alpinists killed worldwide on average every year. Some years such as in 2006, the death toll can be as high as 300 persons killed by avalanches in Europe. There is thus a rising demand for higher safety measures.

For more than a century, scientists have been studying avalanches to try to improve predictions of when they will occur and to optimize defences against them. In the late 19th century, the Swiss forest engineer Johann Coaz started studying snow and monitoring several paths around Davos, which allowed him to publish the first monograph on snow avalanches (Coaz, 1881). Another forest engineer, Paul Mougin, proposed a very simple model in the 1920s to compute avalanche velocity and run-out distance (Mougin, 1922). The model assumes that avalanches behave like sliding blocks. It is still used (in a modified form known as the Voellmy model) by engineers today. A more realistic generation of models, first put forward in the 1970s by Soviet researchers Sergei Grigorian and Margarita Eglit, relies instead on an analogy with flash floods and uses differential equations that describe the motion of water waves (Grigorian *et al.*, 1967).

In spite of substantial progress accomplished over the last century, we still do not know precisely what combination of physical conditions gives rise to avalanches and what exactly governs the way they flow. Our ability to predict when avalanches will occur is limited because the weather conditions that give rise to them are far from clear cut (Schweizer *et al.*, 2003). It is also difficult to construct defences against avalanches because we only have a limited understanding of how they flow. Building walls to either stop or divert avalanches requires a knowledge of how far a potential avalanche is likely to travel, how fast it will be traveling when it reaches the barrier and how broad it will be. Predicting these things is still quite hit and miss.

This chapter summarizes the paramount features of avalanches (formation and motion) and outlines the main approaches used for describing their movement. We do not tackle specific problems related to snow mechanics and

avalanche forecasting. For more information on the subject, the reader is referred to the main textbooks published in Alpine countries (Ancey, 2006; Pudasaini & Hutter, 2006; Amman *et al.*, 1997; Hutter, 1996; McClung & Schaerer, 1993; La Chapelle, 1977).

## 1.1 A physical picture of avalanches

Avalanches are rapid gravity-driven masses of snow moving down mountain slopes. Many, if not most, catastrophic avalanches follow the same basic principle: fresh snow accumulates on the slope of a mountain until the gravitational force at the top of the slope exceeds the binding force holding the snow together. A solid slab of the surface layer of snow can then push its way across the underlying layer, resulting in an avalanche. The failure may also arise from a temperature increase, which reduces snow cohesion. Typically, most avalanches travel for a few hundred meters at a rather low velocity (a few meters per second), but some can move up to 15 km and achieve velocities as high as 100 m/s. They can also pack an incredible punch, up to several atmospheres of pressure.

## 1.2 Avalanche release

Successive snowfalls during the winter and spring accumulate to form snow cover. Depending on the weather conditions, significant changes in snow (types of crystal) occur as a result of various mechanical (creep, settlement) and thermodynamic processes (mass transfer) (Colbeck, 1991; Schweizer *et al.*, 2003). This induces considerable variations in its mechanical properties (cohesion, shear strength). Due to its layer structure, the snow cover is liable to internal slides between layers induced by gravity. When the shear deformation exceeds the maximum value that the layers of snow can undergo, a failure arises, usually developing first along the sliding surface, then propagating throughout the upper layers across a crack perpendicular to the downward direction. This kind of release is very frequent. In the field, evidence of such failures consists of a clear fracture corresponding to the breakaway wall at the top edge of the slab and a bed surface over which the slab has slid (see Fig. 1). If the snow is too loose, the failure processes differ significantly from the ones governing slab release. Loose snow avalanches form near the surface. They usually start from a single point, then they spread out laterally by pushing and incorporating more snow.

The stability of a snow cover depends on many parameters. We can distinguish the fixed parameters related to the avalanche path and the varying parameters, generally connected to weather conditions (Ancey, 1998; de Quervain, 1981; Bernard, 1927). Fixed parameters include:

- *Mean slope.* In most cases, the average inclination of starting zones ranges from  $27^\circ$  to  $50^\circ$ . On rare occasions, avalanches can start on gentle slopes of less than  $25^\circ$  (e.g. *slushflow* involving wet snow with high water content), but generally the shear stress induced by gravity is not large enough to cause failure (Lackinger, 1986). For inclinations in excess of  $45^\circ$  to  $50^\circ$ , many slides (*shuffs*) occur during snowfalls; thus amounts of snow deposited on steep slopes are limited.
- *Roughness.* Ground surface roughness is a key factor in the anchorage of the snow cover to the ground. Dense forests, broken terrain, starting zones



Fig. 1: (a) slab avalanche released by gliding wet snow; note also that single-point releases can also be observed. (b) Dry-snow slab avalanche in the La Sionne field site (courtesy of SLF).

cut by several ridges, ground covered by large boulders generally limit the amount of snow that can be involved in the start of an avalanche. Conversely, widely-spaced forests, large and open slopes with smooth ground facilitate avalanche release.

- *Shape and curvature of starting zone.* The stress distribution within the snowpack and the variation in its depth depend on the longitudinal shape of the ground. For instance, convex slopes concentrate tensile stresses and are generally associated with a significant variation in the snowcover depth, favoring snowpack instability.
- *Orientation to the sun.* The orientation of slopes with respect to the sun has a strong influence on the day-to-day stability of the snowpack. For instance, in winter, shady slopes receive little incoming radiation from the sun and conversely lose heat by long-wave radiation. It is generally observed that for these slopes, the snowpack is cold and tends to develop weak layers (faceted crystals, depth hoar). Many fatalities occur each year in such conditions. In late winter and in spring, the temperature increase enhances stability of snowpacks on shady slopes and instability on sunny slopes.

Among the varying factors intervening in avalanche release, experience clearly shows that in most cases, avalanches result from changes in weather conditions:

- *New snow.* Most of the time, snowfall is the cause of avalanches. The hazard increases significantly with the increase in the depth of new snow. For instance, an accumulation of 30 cm/day may be sufficient to cause widespread avalanching. In European mountain ranges, heavy snowfalls with a total precipitation exceeding 1 m during the previous three days may produce large avalanches, with possible extension down to the valley bottom.
- *Wind.* The wind is an additional factor which significantly influences the stability of a snowpack. Indeed it causes uneven snow redistribution (accumulation on lee slopes), accelerates snow metamorphism, forms cornices, whose collapses may trigger avalanches. On the whole, influence of the wind is very diverse, either consolidating snow (compacting and rounding snow crystals) or weakening it.
- *Rain and liquid water content.* The rain plays a complex role in snow metamorphism. Generally, for dry snow, a small increase in the liquid water content ( $LWC < 0.5\%$ ) does not significantly affect the mechanical properties of snow. However, heavy rain induces a rapid and noticeable increase in LWC, which results in a drop in the shear stress strength. This situation leads to widespread avalanche activity (wet snow avalanches) (Conway & C.F., 1993).
- *Snowpack structure.* A given snowpack results from the successive snowfalls. The stability of the resulting layer structure depends a great deal on the bonds between layers and their cohesion. For instance, heterogeneous snowpacks, made up of weak and stiff layers, are more unstable than homogeneous snowpacks (Schweizer *et al.*, 2003).

### 1.3 Avalanche motion

It is helpful to consider two limiting cases of avalanches depending on the flow features (de Quervain, 1981; Ancey & Charlier, 1996):

- The *flowing avalanche* (avalanche coulante, Fließlawine, valanga radente): a flowing avalanche is an avalanche with a high-density core at the bottom. Trajectory is dictated by the relief. The flow depth does not generally exceed a few meters (see Fig. 2). The typical mean velocity ranges from 5 m/s to 25 m/s. On average, the density is fairly high, generally ranging from 150 kg/m<sup>3</sup> to 500 kg/m<sup>3</sup>.
- The *airborne avalanche* (avalanche en aérosol, Staublawine, valanga nubiforme): it is a very rapid flow of a snow cloud, in which most of the snow particles are suspended in the ambient air by turbulence (see Fig. 3). Relief has usually weak influence on this aerial flow. Typically, for the flow depth, mean velocity, and mean density, the order of magnitude is 10–100 m, 50–100 m/s, 5–50 kg/m<sup>3</sup> respectively.



Fig. 2: Flowing avalanche impacting a wing-shaped structure in the Lauratet experimental site, France (courtesy of O. Marco, Cemagref).

The avalanche classification proposed here only considers the form of motion and not the quality of snow. In the literature, other terms and classifications have been used. For instance, it is very frequent to see terms such as dry-snow avalanches, wet-snow avalanches, powder avalanches, etc. In many cases and probably in most cases in ordinary conditions, the motion form of large avalanches is directly influenced by the quality of snow in the starting zone. For instance, on a sufficiently steep slope, dry powder snow often gives rise to an airborne avalanche (in this case no confusion is possible between airborne and powder snow avalanches). However, in some cases, especially for extreme avalanches (generally involving large volumes of snow), motion is independent of the snow type. For instance, wet snow may be associated with an airborne



Fig. 3: Airborne avalanche at le Roux-d’Abriès, France in 2004 (courtesy of Maurice Chave).

part (e.g. Favrand avalanche in the Chamonix valley, France, on 16 May 1983). Between the two limiting cases above, there is a fairly wide variety of avalanches, which exhibit characteristics common to both airborne and flowing avalanches. Sometimes, such flows are referred to as “mixed-motion avalanches”. The use of this term is often inappropriate because it should be restricted to describing complex flows for which both the dense core and the airborne play a role (from a dynamic point of view). In some cases, the dense core is covered with a snow dust cloud, made up of snow particles suspended by turbulent eddies of air resulting from the friction exerted by the air on the core. This cloud can entirely hide the high-density core, giving the appearance of an airborne avalanche, but in fact, it plays no significant role in avalanche dynamics. It should be born in mind that the mere observation of a cloud is generally not sufficient to specify the type of an avalanche. Further elements such as the features of the deposit or the destructive effects are required.

To conclude it should be noticed that there is currently a limited amount of data on real events. Some of the main parameters, such as the mean density in an airborne avalanche, are still unknown. Thus, many elements of our current knowledge of avalanches have a speculative basis. Today a great deal of work is underway to acquire further reliable data on avalanche dynamics. Experimental sites, such as *la Sionne* (Switzerland) or the *Lautaret pass* (France), have been developed for that purpose. However a survey of extreme past events shows that the characteristics of extreme avalanches (involving very large volumes) cannot be easily extrapolated from the features of ordinary avalanches. In this respect, the situation is not very different from the problems encountered with large rockfalls and landslides (Savage & Hutter, 1989). Many observations that hold for ordinary events no longer hold for rare events. Examples include the role of the forest, the influence of the snow type on avalanche motion, etc.

## 2 Modeling avalanches

Avalanches are extremely complex phenomena. This complexity has led to the development of several approaches based on very different points of view. Many papers and reports have presented an overview of current models. These include the reviews by Hopfinger (1983) and Hutter (1996) as well as a comprehensive review of all existing models edited by Harbitz (1999). Here we shall only outline three typical approaches: the statistical approach, the fluid-mechanics approach, and small-scale models.

### 2.1 Statistical methods

In land-use planning (avalanche zoning), the main concern is to delineate areas subject to avalanches. Avalanche mapping generally requires either accurate knowledge of past avalanche extensions or methods for computing avalanche boundaries. To that end several statistical methods have been proposed (Bovis & Mears, 1976; Lied & Bakkehøi, 1980; McClung, 2001; Meunier & Ancey, 2004; Keylock, 2005; Straub & Grêt-Regamey, 2006; Eckert *et al.*, 2007, 2008).

The two main models used throughout the world are the one developed by Lied & Bakkehøi (1980) and the one developed subsequently by McClung & Lied (1987). Both attempt to predict the extension (stopping position) of the long-return period avalanche for a given avalanche path. Generally, authors have considered avalanches with a return period of approximately 100 years. All these methods rely on the correlations existing between the runout distance and some topographic parameters. They assume that the longitudinal profile of the avalanche path governs avalanche dynamics. The topographic parameters generally include the location of the top point of the starting zone (called point *A*) and a point of deceleration (point *B*) of the path profile where the local slope equals a given angle, most often  $10^\circ$ . The position of the stopping position (point *C*) is described using the angle  $\alpha$ , which is the angle of the line joining the starting and stopping points with respect to the horizontal (see Fig. 4). Likewise,  $\beta$  is the average inclination of the avalanche path between the horizontal and the line joining the starting point *A* to point *B*.

To smooth irregularities in the natural path profile, a regular curve (e.g. a parabola) can be fit to the longitudinal profile.

Statistical methods have so far been applied to flowing avalanches. In principle, nothing precludes using them for airborne avalanches. But in this case, one is faced with the limited amount of data and their poor quality (airborne avalanches are rare and the limits of their deposits are hard to delineate in the field). As an example of statistical models, we indicate the results obtained by Lied & Toppe (1989). Using regression analysis on data corresponding to the longest runout distance observed for 113 avalanche paths in western Norway, these authors have found that

$$\alpha = 0.96\beta - 1.7^\circ. \quad (1)$$

The regression coefficient  $R$  is fairly good ( $R^2 = 0.93$ ) and the standard deviation  $s$  is relatively small ( $s = 1.4^\circ$ ). Table 1 summarizes the values of  $\alpha$  for various mountain ranges.

Many extensions of the early model developed by Lied and Bakkehøi have been proposed over the last twenty years either to tune the model parameters

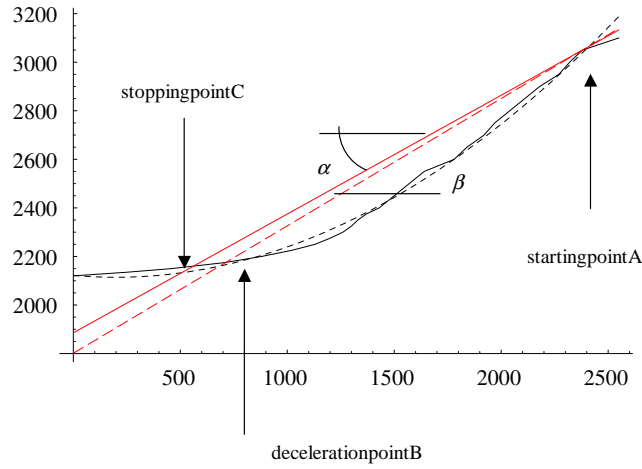


Fig. 4: Topographic parameters describing the profile. The dashed line represents the fit parabola.

Range or contry	$N$	$\alpha$	$R$	$s$
Canada	126	$\alpha = 0.93\beta$	0.86	
Alaska	127	$\alpha = 0.74\beta + 3, 67^\circ$	0.76	
Colorado	52	$\alpha = 0.63\beta + 4, 68^\circ$	0.70	
Sierra Nevada	130	$\alpha = 0.67\beta + 2, 50^\circ$	0.77	
Haute Tarentaise	168	$\alpha = 0.82\beta + 2.82^\circ$	0.81	$2.69^\circ$

Tab. 1: Determination of  $\alpha$  for different mountain ranges.  $N$  refers to the number of sites for each regression analysis. Data collected from (McClung & Mears, 1991; Adjel, 1996).

to a given mountainous region or adapt the computations to other standards. For instance, subsequent work on statistical prediction of avalanche runout distance has accounted for other topographic parameters such as the inclination of the starting zone or the height difference between the starting and deposition zones. Although statistical methods have been extensively used throughout the world over the last twenty years and have given fairly reliable and objective results, many cases exist in which their estimates are wrong. Such shortcomings can be explained (at least in part) by the fact that for some avalanche paths, the dynamic behavior of avalanches cannot be merely related or governed by topographic features (Meunier & Ancey, 2004; Meunier *et al.*, 2004).

## 2.2 Fluid-mechanics approach (avalanche-dynamics models)

Snow avalanches usually take the appearance of viscous fluids flowing down a slope and this observation has prompted the use of fluid-mechanics tools for describing their motion. However, the impediments to a full fluid-mechanics approach are many: a wide range of particle size (often in the  $10^{-3}$  – 1-m range), composition that may change with time and/or position, ill-known boundary conditions (e.g., erodible basal surface) and initial conditions, time-dependent

flows with abrupt changes (e.g., surge front, instabilities along the free surface), etc. Testing the rheometrical properties of samples collected in the field remains difficult. To give examples of materials involved in rapid mass movements, Fig. 5 reports different types of snow observed in avalanche deposits. Because of particle size and thermodynamic alteration (snow is highly sensitive to changes in air temperature), using classic rheometers with these materials does not make sense. All these difficulties pose great challenges in any fluid-mechanics approach for modeling rapid mass movements and have given impetus to extensive research combining laboratory and field experiments, theory, field observation, and numerical simulations (Pudasaini & Hutter, 2006; Ancy, 2007).

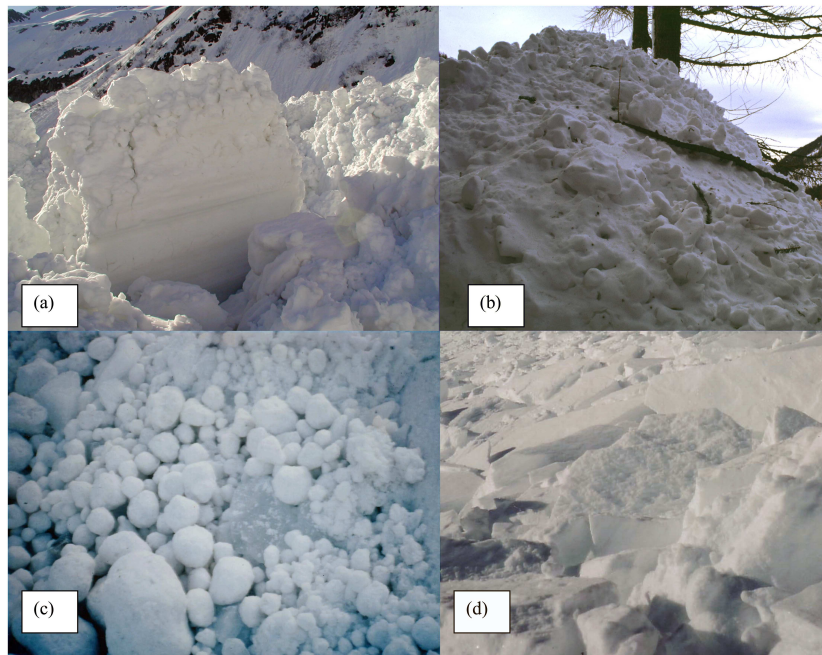


Fig. 5: Different types of snow observed in avalanche deposits. (a) Block of wet snow (size: 1 m). (b) Slurry of dry snow including weak snowballs formed during the course of the avalanche (the heap height was approximately 2 m). (c) Ice balls involved in a huge avalanche coming from the North face of the Mont Blanc (France); the typical diameter was 10 cm. (d) Sintered snow forming broken slabs (typical length: 40 cm, typical thickness 10 cm).

A number of experiments on snow have been done in the laboratory. Authors such as Dent & Lang (1982) and Maeno (1993) have measured the velocity profile within snow flows and generally deduced that snow generates a non-Newtonian viscoplastic flow, whose properties depend a great deal on density. Carrying these laboratory results over real avalanches is not clearly reliable due to size-scale effects and similarity conditions. Furthermore, given the severe difficulties inherent to snow rheometry (sample fracture during shearing tests, variation in the snow microstructure resulting from thermodynamic transformations of crys-

tals, etc.), properly identifying the constitutive equation of snow with modern rheometers is out of reach for the moment. More recently, Ancey & Meunier (2004) showed how avalanche-velocity records can be used to determine the bulk frictional force; a striking result is that the bulk behavior of most snow avalanches can be approximated using a Coulomb frictional model. Kern *et al.* (2004) and Kern *et al.* (2009) used outdoor and field experiments to measure shear-rate profiles inside snow flows to infer rheological properties; this is rather encouraging and clears the way for precise rheometrical investigations of real snow avalanches.

Since there are little sound field or laboratory data available on the basic rheological processes involved in avalanche release and flow, all avalanche-dynamics models proposed so far rely on analogy with other physical phenomena: typical examples include analogies with granular flows (Savage & Hutter, 1989; Savage, 1989; Tai *et al.*, 2001; Cui *et al.*, 2007), Newtonian fluids (Hunt, 1994), power-law fluids (Norem *et al.*, 1986), and viscoplastic flows (Dent & Lang, 1982; Ancey, 1994). From a purely rheological point of view, these models rely on a purely speculative foundation. Indeed, most of the time, the rheological parameters used in these models have been estimated by matching the model predictions (such as the leading-edge velocity and the run-out distance) with field data (Buser & Frutiger, 1980; Dent & Lang, 1980; Ancey *et al.*, 2004). However, this obviously does not provide evidence that the constitutive equation is appropriate.

Avalanches can be considered at different spatial scales (see Fig. 6). The larger scale, corresponding to the entire flow, leads to the simplest models. The chief parameters include the location of the gravity center and its velocity. Mechanical behavior is mainly reflected by the friction force  $F$  exerted by the bottom (ground or snowpack) on the avalanche. The smallest scale, close to the size of snow particles involved in the avalanches, leads to complicated rheological and numerical problems. The flow characteristics (velocity, stress) are computed at any point of the occupied space. Intermediate models have also been developed. They benefit from being less complex than three-dimensional numerical models and yet more accurate than simple ones. Such intermediate models are generally obtained by integrating the motion equations across the flow depth in a way similar to what is done in hydraulics for shallow water equations.

## 2.3 Simple models

Simple models have been developed for almost 80 years in order to crude estimations of avalanche features (velocity, pressure, runout distance). They are used extensively in engineering throughout the world. Despite their simplicity and approximate character, they can provide valuable results, the more so as their parameters and the computation procedures combining expert rules and scientific basis have benefited from many improvements over the last few decades (Ancey *et al.*, 2003; Ancey & Meunier, 2004; Ancey *et al.*, 2004; Ancey, 2005).

### 2.3.1 Simple models for flowing avalanches

The early models date back to the beginning of the 20<sup>th</sup> century (Mougin, 1922). For the Olympic Games at Chamonix in 1924, the Swiss professor Lagotala

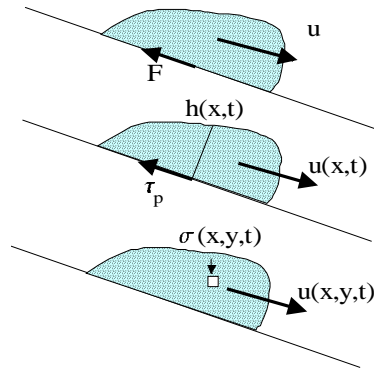


Fig. 6: Different spatial scales used for describing avalanches

(1927) computed the velocity of avalanches in the Favrand path. His method was then extended by Voellmy (1955), who popularized it. Many models have elaborated on Voellmy's work. The Voellmy–Salm–Gubler (VSG) model and the Perla–Cheng–McClung model are probably the best-known avalanche-dynamics models used throughout the world (Salm *et al.*, 1990; Perla *et al.*, 1980).

Here we outline the VSG model developed by Salm *et al.* (1990). The avalanche is assumed to behave as a rigid body, which moves along an inclined plane. The position of the center of mass is given by its abscissa  $x$  in the downward direction. The momentum equation is

$$\frac{du}{dt} = g \sin \theta - \frac{F}{m}, \quad (2)$$

with  $m$  the avalanche mass,  $u$  its velocity,  $\theta$  the mean slope of the path, and  $F$  the frictional force. In this model, a flowing avalanche is considered as a sliding block subject to a frictional force combining a solid-friction component and a square-velocity component:

$$F = mg \frac{u^2}{\xi h} + \mu m g \cos \theta, \quad (3)$$

with  $h$  the mean flow depth of the avalanche,  $\mu$  a friction coefficient related to the snow fluidity, and  $\xi$  a coefficient of dynamic friction related to path roughness. If these last two parameters cannot be measured directly, they can be adjusted from several series of past events. It is generally accepted that the friction coefficient  $\mu$  only depends on the avalanche size and ranges from 0.4 (small avalanches) to 0.155 (very large avalanches) (Salm *et al.*, 1990); in practice, lower values can be observed for large-volume avalanches (Ancey *et al.*, 2004). Likewise, the dynamic parameter  $\xi$  reflects the influence of the path on avalanche motion. When an avalanche runs down a wide open rough slope,  $\xi$  is close to 1000 or more. Conversely, for avalanches moving down confined straight gullies,  $\xi$  can be taken as being equal to 400. In a steady state, the velocity is directly inferred from the momentum balance equation:

$$u = \sqrt{\xi h \cos \theta (\tan \theta - \mu)}. \quad (4)$$

According to this equation two flow regimes can occur depending on path inclination. For  $\tan \theta > \mu$ , (4) has a real solution and a steady regime can occur. For  $\tan \theta < \mu$ , there is no real solution: the frictional force (3) outweighs the downward component of the gravitational force. It is therefore considered that the flow slows down. The point of the path for which  $\tan \theta = \mu$  is called the characteristic point (point  $P$ ). It plays an important role in avalanche dynamics since it separates flowing and runout phases. In the stopping area, we deduce from the momentum equation that the velocity decreases as follows:

$$\frac{1}{2} \frac{du^2}{dx} + u^2 \frac{g}{\xi h} = g \cos \theta (\tan \theta - \mu) . \quad (5)$$

The runout distance is easily inferred from (5) by assuming that at a point  $x = 0$ , the avalanche velocity is  $u_p$ . In practice the origin point is point  $P$  but attention must be paid in the fact that, according to (4), the velocity at point  $P$  should be vanishing; a specific procedure has been developed to avoid this shortcoming (Salm *et al.*, 1990). Neglecting the slope variations in the stopping zone, we find:

$$x_a = \frac{\xi h}{2g} \ln \left( 1 + \frac{u_p^2}{\xi h \cos \theta (\mu - \tan \theta)} \right) . \quad (6)$$

This model enables us to easily compute the runout distance, the maximum velocities reached by the avalanche on various segments of the path, the flow depth (by assuming that the mass flow rate is constant and given by the initial flow rate just after the release), and the impact pressure.

Ancey & Meunier (2004) performed a back analysis on 15 well-documented avalanches by inferring the bulk frictional force from avalanche velocity. To that end, they used (2): if one has a record yielding the body velocity as a function of the position along the path, then it is possible to directly deduce the frictional force components and its relationship with the velocity  $u$  to a multiplicative factor  $m$ . Plotting the resulting force per unit mass in a phase space ( $u, F/m$ ) can give an idea of the dependence of the frictional force on mean velocity.

For most events, the frictional force was found to be weakly dependent on velocity or to fluctuate around a mean value during the entire course of the avalanche. Figure 7 shows a typical example provided by the avalanche at the Arraba site (Italy) on 21 December 1997. This figure reports the variation in the frictional force per unit mass with velocity (solid line) and the downward component of the driving force per unit mass  $g \sin \theta$  (dashed line). In the inset, we have plotted the measured velocities (dots) together with its interpolation curve (Legendre polynomials) used in the computations. On the same plot, we have drawn the velocity variations as if the avalanche were in a purely Coulomb regime (dashed line): assuming that the frictional force is in the Coulomb form  $F = fmg \cos \theta$ , where  $f$  is the bulk friction coefficient, we numerically solved the equation of motion (Eq. 2, in which  $F/m$  is replaced with the expression of  $F$  above). As shown in Fig. 7, in the early phases (between points A and B), the frictional force gently decreased with increasing velocity and was slightly lower than the gravity acceleration  $g \sin \theta$ . Because of the small difference between  $g \sin \theta$  and  $F/m$ , the avalanche accelerated less vigorously than an avalanche in an inertial regime. At instant B, the avalanche reached its maximum velocity (24 m/s). At this point, the frictional force started exceeding the gravitational force and the avalanche decelerated monotonically. Obviously, the frictional force did

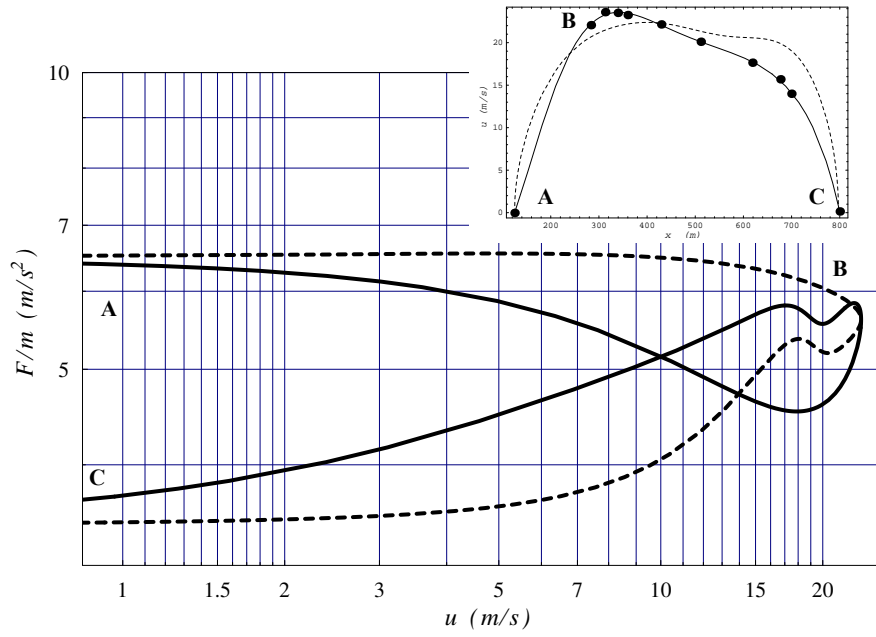


Fig. 7: Variation in the frictional force per unit mass  $F/m$  with the avalanche velocity  $u$  for the avalanche of 21 December 1997 at the Arabba site (solid line);  $F/m$  was obtained by applying Eq. (2) to the measured velocities and path profile, both regularized using Legendre polynomials. The dashed curve stands for the variation in the driving force per unit mass  $g \sin \theta$ . In the inset, we have reported the variations in the measured velocities (dots) with downstream distance  $x$ . In the inset, the solid line represents the interpolated velocities while the dashed line stands for the velocity of a rigid body sliding in a purely Coulomb regime (with  $f = 0.66$ ). Letters from A to C refer to various stages of the avalanche run (see text). After Ancey & Meunier (2004).

depend on the avalanche velocity, as shown in Fig. 4, but this dependence remained slight since between B and C we have:  $F/m \propto u^{0.1 \pm 0.05}$ . Thus, as a first approximation, the frictional force can be considered constant between instants A and C:  $F/m = 5 \pm 1.3 \text{ m/s}^2$ . As shown in the inset of Fig. 7, the computed velocities obtained by assuming a purely Coulomb regime (dashed curve) compare well with the data: like the recorded values, the computed velocities exhibit an asymmetric U-shaped form, while the relative deviation between the two curves is less than 20%.

For a few events, the bulk frictional force exhibits a dependence on the mean velocity, but no clear trend in the  $f(u)$  dependence was found by Ancey & Meunier (2004). An interesting property of this simple Coulomb block model is that knowing the run-out distance (point of furthest reach) of an avalanche makes it possible to infer the  $f$  value. Since in different alpine regions, avalanche events have been recorded over a long time period at different sites, we can deduce the statistical properties of the  $f$  distribution at different places. If the bulk friction coefficient  $f$  were a true physical parameter, its statistical properties should not vary with space. Ancey (2005) thus conducted a statistical analysis on  $f$  values by selecting 173 avalanche data collected from seven sites in France. These sites are known to produce large avalanches and their activity has been followed up since the beginning of the 20th century. Figure 8 shows the probability distribution of  $f$  for each site together with the entire sample. Although the curves are close and similar, they are not statistically identical. This means that the probability distribution function of  $f$  is not uniquely determined and depends on other parameters such as snow properties, site configuration, etc. Within this approach, the Coulomb model successfully captures the flow features, but its friction parameter is not a true physical parameter. This, however, should not negate the interest of the Coulomb model because, given the number of approximations underpinning the sliding-block model, the statistical deviance may originate from crude assumptions.

### 2.3.2 Simple models for airborne avalanches

The first-generation models of airborne avalanches used the analogy of density currents along inclined surfaces. Extending a model proposed by Ellison & Turner (1959) on the motion of an inclined plume, Hopfinger & Tochon-Danguy (1977) inferred the mean velocity of a steady current, assumed to represent the avalanche body behind the head. They found that the front velocity of the current was fairly independent of the bed slope. Further important theoretical contributions to modeling steady density currents were provided by Parker *et al.* (1986) and Baines (2001). The second generation of models has considered the avalanche as a finite-volume turbulent flow of a snow suspension. Kulikovskiy & Svehnikova (1977) set forth a fairly simple theoretical model (the KS model), in which the cloud was assimilated to a semi-elliptic body whose volume varied with time. The kinematics was entirely described by the mass center position and two geometric parameters of the cloud (the two semi-axes of the ellipsis). The cloud density can vary depending on air and snow entrainments. Kulikovskiy and Sveshnikova obtained a set of four equations describing the mass, volume, momentum, and Lagrangian kinetic energy balances. The idea was subsequently redeveloped by many authors including Beghin (1979), Beghin *et al.* (1981), Beghin & Brugnot (1983), Fukushima & Parker (1990), Beghin & Olagne (1991),

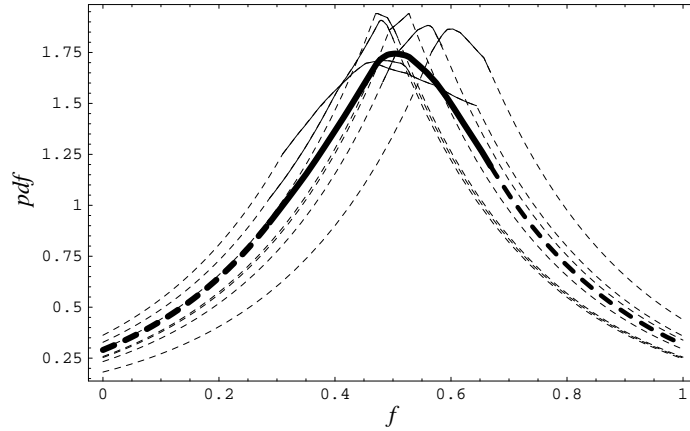


Fig. 8: Empirical probability distribution functions (pdf) of the 173  $f$  values collected from the seven paths. The thick line represents the distribution function of the total sample, whereas the thin lines are related to individual paths. Each curve has been split into three parts: the central part (solid line) corresponds to the range of computed  $\mu$  values, while the end parts have been extrapolated. After Ancey (2005).

Fukushima *et al.* (2000), Ancey (2004), and Turnbull *et al.* (2007).

Here we outline the KSB model as presented and extended by Ancey (2004), we will consider the two-dimensional motion of a cloud along a plane inclined at an angle  $\tan \theta$  with respect to the horizontal. Figure 9 depicts a typical cloud entraining particles from the bed. In the following,  $H$  denotes the cloud height,  $L$  its length,  $m$  its mass,  $V$  its volume. The cloud velocity is  $U = dx/dt$  but, since the body is deformable, the velocity varies inside the body. The front position is given by the abscissa  $x_f$  while its velocity is  $U_f = dx_f/dt$ . The volume solid concentration is  $\phi$  and it is assumed that the cloud is a homogeneous suspension of particles of density  $\rho_p$  (no density stratification) in the ambient fluid of density  $\rho_a$  and viscosity  $\mu_a$ . The bulk cloud density is then:  $\bar{\rho} = \phi\rho_p + (1 - \phi)\rho_a$ . Ahead of the front, there is a particle bed whose thickness is denoted by  $h_n$ , and which is made up of the same particles as the cloud. The apparent density of the layer is  $\rho_s = \phi_m\rho_p + (1 - \phi_m)\rho_a$ , where  $\phi_m$  denotes the maximum random volume concentration of particles.

The surface area (per unit width) exposed to the surrounding fluid is denoted by  $S$  and can be related to  $H$  and  $L$  as follows:  $S = k_s\sqrt{HL}$ , where  $k_s$  is a shape factor. Here we assume that the cloud keeps a semi-elliptic form, whose aspect ratio  $k = H/L$  remains constant during the cloud run when the slope is constant. We then obtain

$$k_s = E(1 - 4k^2)/\sqrt{k}, \quad (7)$$

where  $E$  denotes the elliptic integral function. Similarly, we can also express the volume  $V$  (per unit width) as:  $V = k_vHL$ , where  $k_v$  is another shape factor for a half ellipsis. Here we have

$$k_v = \pi/4. \quad (8)$$

In the following, we will also need to use the volume, height, and length growth

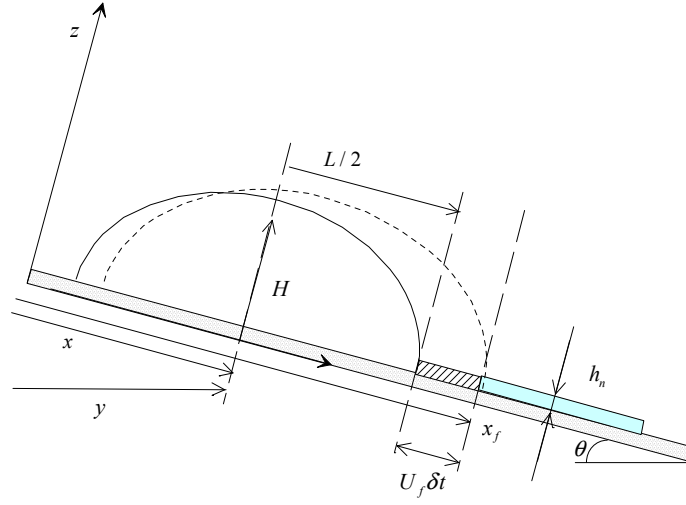


Fig. 9: Sketch of the physical system studied here.

rates:

$$\alpha_v = \frac{1}{\sqrt{V}} \frac{dV}{dx}, \quad \alpha_h = \frac{dH}{dx}, \quad \alpha_l = \frac{dL}{dx}. \quad (9)$$

Experimentally, it is easier to measure the growth rates by deriving the quantity at hand by the front abscissa instead of the mass center abscissa; we will refer to these rates as:

$$\tilde{\alpha}_v = \frac{1}{\sqrt{V}} \frac{dV}{dx_f}, \quad \tilde{\alpha}_h = \frac{dH}{dx_f}, \quad \tilde{\alpha}_l = \frac{dL}{dx_f}. \quad (10)$$

Note that all these quantities are interrelated. For instance, using  $x = x_f - L/2$ , we find:  $\tilde{\alpha}_h = (dH/dx)(dx/dx_f) = \alpha_h(1 - \tilde{\alpha}_l/2)$ . Similarly, using the definition of  $k$  and  $k_v$ , we obtain:

$$\alpha_h = \frac{\alpha_v}{2} \sqrt{\frac{k}{k_v}} \quad \text{and} \quad \alpha_l = \frac{\alpha_v}{2\sqrt{k k_v}}. \quad (11)$$

The KSB model outlined here includes three equations: volume, mass, and momentum balances. The volume variations mainly result from the entrainment of the ambient, less dense fluid. Various mixing processes are responsible for the entrainment of the ambient fluid into the cloud. It has been shown for jets, plumes, and currents that (i) different shear instabilities can occur at the interface between dense and less dense fluids, (ii) the rate of growth of these instabilities is controlled by a Richardson number, defined here :

$$Ri = \frac{g' H \cos \theta}{U^2}, \quad (12)$$

where  $g'$  denotes the reduced gravity  $g' = g\Delta\bar{\rho}/\rho_a$  and  $\Delta\bar{\rho} = \bar{\rho} - \rho_a$  is the buoyant density.

Usually a smaller  $Ri$  value implies predominance of inertia effects over the restoring action of gravity, thus greater instability and therefore a higher entrainment rate; it is then expected that the entrainment rate is a decreasing

function of the Richardson number. Although the details of the mixing mechanisms are very complex, a striking result of recent research is that their overall effects can be described in quite a simple way (Fernando, 1991). To express the volume balance equation, the commonest assumption is to state that the volume variations come from the entrainment of the ambient fluid into the cloud and that the inflow rate is proportional to the exposed surface area and a characteristic velocity  $u_e$ . This leads to the equation:

$$\frac{dV}{dt} = E_v S u_e \quad (13)$$

where  $E_v$  is the bulk entrainment coefficient. According to the flow conditions, different expressions of  $E_v$  have been drawn from experiments. Interestingly enough, the value of  $E_v$  has been expressed very differently depending on whether the current is steady or unsteady. There is, however, no clear physical reason justifying this partitioning. Indeed, for most experiments, the currents were gradually accelerating and mixing still occurred as a result of the development of Kelvin-Helmoltz billows, thus very similarly to the steady case. This prompted Ancy (2004) to propose a new expression of the entrainment coefficient for clouds, which holds for both steady and slightly unsteady conditions: Ancy (2004) related  $E_v$  (or  $\alpha_v$ ) as a function of  $Ri$  (instead of  $\theta$  as done by previous authors): for  $Ri \leq 1$ ,  $\alpha_v = e^{-1.6Ri^2}$  while for  $Ri > 1$ ,  $\alpha_v = 0.2/Ri$ .

The cloud mass can vary as a result of the entrainment of the surrounding fluid and/or the entrainment of particles from the bed. The former process is easily accounted for: during a short time increment  $\delta t$ , the cloud volume  $V$  is increased by a quantity  $\delta V$  mainly as a result of the air entrainment, thus the corresponding increase in the cloud mass is  $\rho_a \delta V$ . The latter process is less well known. In close analogy with sediment erosion in rivers and turbidity currents, (Fukushima & Parker, 1990) assumed that particles are continuously entrained from the bed when the drag force exerted by the cloud on the bed exceeds a critical value. This implies that the particle entrainment rate is controlled by the surface of the bed in contact with the cloud and the mismatch between the drag force and the threshold of motion. Here, since in extreme conditions the upper layers of the snowcover made up of new snow of weak cohesion can be easily entrained, it is reasonable to think that all the recent layer ahead of the cloud is incorporated into the cloud: when the front has traveled a distance  $U_f \delta t$ , where  $U_f$  is the front velocity, the top layer of depth  $h_n$  and density  $\rho_s$  is entirely entrained into the cloud (see Fig. 9). The resulting mass variation (per unit width) is written:  $\rho_s U_f h_n \delta t$ . At the same time, particles settle with a velocity  $v_s$ . During the time step  $\delta t$ , all the particles contained in the volume  $L v_s \delta t$  deposit. Finally, by taking the limit  $\delta t \rightarrow 0$ , we can express the mass balance equation as follows:

$$\frac{dm}{dt} = \rho_a \frac{dV}{dt} + \rho_s U_f h_n - \phi \rho_s L v_s$$

where  $m = \bar{\rho} V$  is the cloud mass. Usually the settling velocity  $v_s$  is very low compared to the mean forward velocity of the front so that it is possible to ignore the third term in the right-hand side of the equation above. We then obtain the following simplified equation:

$$\frac{d\Delta \bar{\rho} V}{dt} = \rho_s U_f h_n \quad (14)$$

The cloud undergoes the driving action of gravity and the resisting forces due to the ambient fluid and the bottom drag. The driving force per unit volume is  $\bar{\rho}g \sin \theta$ . Most of the time, the bottom drag effect plays a minor role in the accelerating and steady-flow phases but becomes significant in the decelerating phase (Hogg & Woods, 2001). Since we have set aside a number of additional effects (particle sedimentation, turbulent kinetic energy), it seems reasonable to also discard this frictional force. The action of the ambient fluid can be broken into two terms: a term analogous to a static pressure (Archimede's theorem), equal to  $\rho_a V g$ , and a dynamic pressure. As a first approximation, the latter term can be evaluated by considering the ambient fluid as an inviscid fluid in an irrotational flow. On the basis of this approximation, it can be shown that the force exerted by the surrounding fluid on the half cylinder is  $\rho_a V \chi dU/dt$ , where

$$\chi = k \quad (15)$$

is called the *added mass coefficient*. Since at the same time volume  $V$  varies and the relative motion of the half cylinder is parallel to its axis of symmetry, we finally take:  $\rho_a \chi d(UV)/dt$ . Note that this parameter could be ignored for light interstitial fluids (e.g., air), whereas it has a significant influence for heavy interstitial fluids (basically water). Thus the momentum balance equation can be written as:

$$\frac{d(\bar{\rho} + \chi \rho_a) V U}{dt} = \Delta \bar{\rho} g V \sin \theta \quad (16)$$

Analytical solutions can be found in the case of a Boussinesq flow ( $\bar{\rho}/\rho_a \rightarrow 1$ ); for the other cases, numerical methods must be used. In the Boussinesq limit, since the final analytical solution is complicated, we only provide an asymptotic expression at early and late times. To simplify the analytical expressions, without loss of generality, here we take:  $U_0 = 0$  and  $x_0 = 0$  and we assume that the erodible snowcover thickness  $h_n$  and density  $\rho_s$  are constant. The other initial conditions are: at  $t = 0$  and  $x = 0$ ,  $H = H_0$ ,  $L = L_0$ ,  $V_0 = k_v H_0 L_0$ , and  $\bar{\rho} = \bar{\rho}_0$ . At short times, the velocity is independent of the entrainment parameters and the initial conditions ( $\bar{\rho}_0$  and  $V_0$ ):

$$U \propto \sqrt{2gx \sin \theta \frac{\Delta \rho_0}{\Delta \rho_0 + (1 + \chi) \rho_a}} \approx \sqrt{2gx \sin \theta} \quad (17)$$

where we used  $\rho_a \ll \Delta \bar{\rho}_0$ . This implies that the cloud accelerates vigorously in the first instants ( $dU/dx \rightarrow \infty$  at  $x = 0$ ), then its velocity grows more slowly. At long times for an infinite plane, the velocity reaches a constant asymptotic velocity that depends mainly on the entrainment conditions for flows in the air:

$$U_\infty \propto \sqrt{\frac{2gh_n(1 + \frac{\alpha_v}{2}) \sin \theta \rho_s}{\alpha_v^2(1 + \chi) \rho_a}} \quad (18)$$

Because of the slow growth of the velocity, this asymptotic velocity is reached only at very long times. Without particle entrainment, the velocity reaches a maximum at approximately  $x_m^2 = (2\rho_0/3\rho_a)\alpha_v^{-2}V_0/(1 + \chi)$ :

$$U_m^2 \approx \frac{4}{\sqrt{3}} \sqrt{\frac{\rho_0}{\rho_a} \frac{g \sqrt{V_0} \sin \theta}{\alpha_v \sqrt{1 + \chi}}}$$

then it decreases asymptotically as:

$$U \propto \sqrt{\frac{8\Delta\rho_0 gV_0 \sin\theta}{3\rho_a} \frac{1}{x} \frac{1}{\alpha_v^2(1+\chi)}} \quad (19)$$

In this case, the front position varies with time as:

$$x_f \propto (g'_0 V_0 \sin\theta)^{1/3} t^{2/3} \quad (20)$$

These simple calculations show the substantial influence of the particle entrainment on cloud dynamics. In the absence of particle entrainment from the bed, the fluid entrainment has a key role since it directly affects the value of the maximum velocity that a cloud can reach.

Here, we examine only the avalanche of 25 February 1999, for which the front velocity was recorded (Dufour *et al.*, 2001). In Fig. 10, we have reported the variation in the mean front velocity  $U_f$  as a function of the horizontal downstream distance  $y_f$ : the dots correspond to the measured data while the curves represent the solution obtained by integrating Eqs. (13–16) numerically and by assuming that the growth rate coefficient depends on the overall Richardson number (solid line). For the initial conditions, we assume that  $u_0 = 0$ ,  $h_0 = 2.1$  m  $l_0 = 20$  m, and  $\rho_0 = \rho_s = 150$  kg/m<sup>3</sup>. Due to the high path gradient between the origin and the elevation  $z = 1800$  m ( $y = 1250$  m) we have considered that on average, the released snow layer  $h_n$  is 0.7 m thick and is entirely entrained into the avalanche. Using  $\alpha_v \propto Ri^{-1}$  for  $Ri \gg 1$ , we apply the following relationship: for  $Ri \leq 1$ ,  $\alpha_v = e^{-1.6Ri^2}$  while for  $Ri > 1$ , we take  $\alpha_v = 0.2/Ri$ .

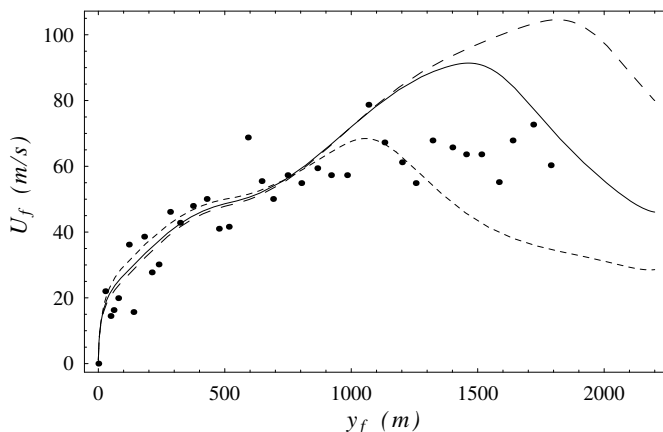


Fig. 10: Dependence of the front velocity on the erodible mass. Solid line:  $\rho_s h_n = 105$  kg/m<sup>2</sup>; dashed line:  $\rho_s h_n = 50$  kg/m<sup>2</sup>; long-dashed line:  $\rho_s h_n = 150$  kg/m<sup>2</sup>. After (Ancey, 2004).

As shown in Fig. 10, the avalanche accelerated vigorously after the release and reached velocities as high as 80 m/s. The velocity variation in the release phase is fairly well described by the KSB model. The model predicts a bell-shaped velocity variation while field data provide a flatter velocity variation. The computed flow depth at  $z = 1640$  m is approximately 60 m which is consistent with the value estimated from the video tapes. In order to evaluate the

sensitivity of the simulation results, we examined different values of the erodible mass. In Figure 10, we have reported the comparison between field data and computations made with three different assumptions:  $\rho_s h_n = 50, 105,$  or  $150 \text{ kg/m}^2$ . It can be seen that there is no significant variation in the computed velocities in the accelerating phase, but both the maximum velocity and the position at which the maximum velocity is reached depend on the  $\rho_s h_n$  value. By increasing the erodible mass per unit surface from 50 to  $150 \text{ kg/m}^2$ , the maximum velocity is increased from 69 m/s to 105 m/s, i.e., by a factor of 1.5. Note that the dependence of the maximum velocity on the snowcover thickness is consistent with field measurements made by Dufour *et al.* (2001): for instance, the avalanche of 10 February 1999 was approximately half as large in terms of deposited volume as the avalanche of 25 February 1999, and its maximum velocity was 25% lower than the maximum velocity recorded on 25 February 1999. This result is of great importance in engineering applications since it means that the maximum velocity and, thereby, the destructive power of a powder-snow avalanche mainly result from the ability to entrain snow from the snowcover when the avalanche descends.

## 2.4 Intermediate models (depth-averaged models)

Simple models can provide approximate predictions concerning runout distance, the impact pressure, or deposit thickness. However they are limited for many reasons. For instance, they are restricted to one-dimensional path profiles (the spreading of the avalanche cannot be computed) and the parameters used are fit to past events and cannot be measured in the field or in the laboratory (rheometry), apart from airborne models if the analogy with turbidity currents is used. More refined models use depth-averaged mass and momentum equations to compute the flow characteristics. With such models, the limitations of simple models are alleviated. For instance it is possible to compute the spreading of avalanches in their runout zone or relate mechanical parameters used in the models to the rheological properties of snow. As far as we know, the early depth-averaged models were developed in the 1970s by Russian scientists (Bozhinskiy & Losev, 1998) and French researchers (Brugnot & Pochat, 1981; Vila, 1986) for flowing avalanches. For airborne avalanches, the first stage was probably the model developed by Parker *et al.* (1986), which, though devoted to submarine turbidity currents, contains almost all the ingredients used in subsequent models of airborne avalanches. Considerable progress in the development of numerical depth-averaged models has been made possible thanks to the increase in computer power and breakthrough in the numerical treatment of hyperbolic partial differential equation systems (LeVeque, 2002).

### 2.4.1 Depth-averaged motion equations

Here, we shall address the issue of slightly transient flows. We focus exclusively on *gradually varied flows*, namely flows that are not far from a steady uniform state for the time interval under consideration. Moreover, we first consider flows without entrainment of the surrounding fluid and variation in density:  $\varrho \approx \bar{\varrho}$ . Accordingly the bulk density may be merely replaced by its mean value. In this context, the motion equations may be inferred in a way similar to the usual procedure used in hydraulics to derive the shallow water equations

(or Saint–Venant equations): it involves integrating the momentum and mass balance equations over the depth. As such a method has been extensively used in hydraulics for water flow (Chow, 1959) as well for non-Newtonian fluids (Savage & Hutter, 1991; Bouchut *et al.*, 2003); we shall briefly recall the principle and then directly provide the resulting motion equations. Let us consider the local mass balance:  $\partial \varrho / \partial t + \nabla \cdot (\varrho \mathbf{u}) = 0$ . Integrating this equation over the flow depth leads to:

$$\int_0^{h(x,t)} \left( \frac{\partial u}{\partial x} + \frac{\partial v}{\partial y} \right) dy = \frac{\partial}{\partial x} \int_0^h u(x, y, t) dy - u(h) \frac{\partial h}{\partial x} - v(x, h, t) - v(x, 0, t), \quad (21)$$

where  $u$  and  $v$  denote the  $x$ - and  $y$ -component of the local velocity. At the free surface and the bottom, the  $y$ -component of velocity satisfies the following boundary conditions:

$$v(x, h, t) = \frac{dh}{dt} = \frac{\partial h}{\partial t} + u(x, h, t) \frac{\partial h}{\partial x}, \quad (22)$$

$$v(x, 0, t) = 0. \quad (23)$$

We easily deduce:

$$\frac{\partial h}{\partial t} + \frac{\partial h \bar{u}}{\partial x} = 0, \quad (24)$$

where we have introduced depth-averaged values defined as:

$$\bar{f}(x, t) = \frac{1}{h(x, t)} \int_0^{h(x,t)} f(x, y, t) dy. \quad (25)$$

The same procedure is applied to the momentum balance equation:  $\varrho d\mathbf{u}/dt = \varrho \mathbf{g} + \nabla \cdot \boldsymbol{\sigma}$ , where  $\boldsymbol{\sigma}$  denotes the stress tensor. Without difficulty, we can deduce the averaged momentum equation from the  $x$ -component of the momentum equation:

$$\bar{\varrho} \left( \frac{\partial h \bar{u}}{\partial t} + \frac{\partial h \bar{u}^2}{\partial x} \right) = \bar{\varrho} g h \sin \theta + \frac{\partial h \bar{\sigma}_{xx}}{\partial x} - \tau_p, \quad (26)$$

where we have introduced the bottom shear stress:  $\tau_p = \sigma_{xy}(x, 0, t)$ . In the present form, the motion equation system (24)–(26) is not closed since the number of variables exceeds the number of equations. A common approximation involves introducing a parameter (sometimes called the Boussinesq momentum coefficient) which links the mean velocity to the mean square velocity:

$$\bar{u}^2 = \frac{1}{h} \int_0^h u^2(y) dy = \alpha \bar{u}^2. \quad (27)$$

Usually  $\alpha$  is set to unity, but this may cause trouble when computing the head structure (Hogg & Pritchard, 2004; Ancy *et al.*, 2006, 2007). A point often neglected is that the shallow-flow approximation is in principle valid for flow regimes that are not too far away from a steady-state uniform regime. In flow parts where there are significant variations in the flow depth (e.g. at the leading

edge and when the flow widens or narrows substantially), corrections should be made to the first-order approximation of stress. Recent studies however showed that errors made with the shallow-flow approximation for the leading edge are, however, not significant (Ancey *et al.*, 2007; Ancey & Cochard, 2009; Ancey *et al.*, 2009).

#### 2.4.2 Flowing avalanches

As discussed in the introduction of this section (see Fig. 5), the diversity in snow consistency makes any thorough rheometrical examination of snow involved in avalanches a tricky undertaking. Authors who studied the rheological bulk behavior of snow, have generally found that snow is a non-Newtonian viscoplastic material, which depends a great deal on density. Several constitutive equations have been proposed: Newtonian fluid, Reiner–Ericksen fluid, Bingham fluid, frictional Coulomb fluid, and so on. For instance, Savage and Hutter assumed that flowing avalanches have many similarities with dry granular flows (Savage, 1989; Savage & Hutter, 1991). They have further assumed that, as a first approximation, the Coulomb law can be used to describe the bulk behavior of flowing granular materials. Therefore they have expressed the bottom shear stress as:  $\tau_p = \rho gh \tan \delta \cos \theta$ , where  $\delta$  denotes a bed friction angle. Likewise, the normal mean shear stress can be written as:  $\bar{\sigma}_{xx} = -k_a \rho gh \cos \theta / 2$ , where the coefficient  $k_a$  is related to the earth pressure coefficient used in soil mechanics. Eventually they obtained for flows down inclined planes:

$$\frac{\partial h}{\partial t} + \frac{\partial h \bar{u}}{\partial x} = 0, \quad (28)$$

$$\frac{\partial \bar{u}}{\partial t} + \bar{u} \frac{\partial \bar{u}}{\partial x} = g \cos \theta (\tan \theta - \tan \delta) - k_a g \cos \theta \frac{\partial h}{\partial x}. \quad (29)$$

Laboratory tests with dry granular media have shown that such a model captures the flow features well for steep smooth inclined channels (Savage, 1989; Savage & Hutter, 1989; Hutter *et al.*, 1995, 1993; Gray *et al.*, 1998, 2003; Hákonardóttir & Hogg, 2005). Similar models were developed using different constitutive equations. For instance, Eglit used empirical expressions for the bottom shear stress (in a form similar to (3)) and treated the leading edge using a specific boundary condition (Eglit, 1983, 1998).

#### 2.4.3 Airborne avalanches

An airborne avalanche is a very turbulent flow of a dilute ice–particle suspension in air. It can be considered as a one-phase flow as a first approximation. Indeed, the Stokes number defined as the ratio of a characteristic time of the fluid to the relaxation time of the particles is low, implying that particles adjust quickly to changes in the air motion. At the particle scale, fluid turbulence is high enough to strongly shake the mixture since the particle size is quite small. To take into account particle sedimentation, authors generally consider airborne avalanches as turbulent stratified flows. Thus, contrary to flowing avalanches, bulk behavior is well identified in the case of airborne avalanches. The main differences between the various models proposed result from the different boundary conditions, use of the Boussinesq approximation, and the closure equations for turbulence. Parker *et al.* (1986) developed a complete depth-averaged model for

turbidity currents. The motion equation set proposed by these authors is more complicated than the corresponding set for dense flows presented above, since it includes additional equations arising from the mass balance for the dispersed phase, the mean and turbulent kinetic energy balances, and the boundary conditions related to the entrainment of sediment and surrounding fluid:

$$\frac{\partial h}{\partial t} + \frac{\partial hu}{\partial x} = E_a u, \quad (30)$$

$$\frac{\partial(Ch)}{\partial t} + \frac{\partial(hUC)}{\partial x} = v_s E_s - v_s c_b, \quad (31)$$

$$\frac{\partial hu}{\partial t} + \frac{\partial hu^2}{\partial x} = RCgh \sin \theta - \frac{1}{2} Rg \frac{\partial Ch^2}{\partial x} - u_*^2, \quad (32)$$

$$\frac{\partial hK}{\partial t} + \frac{\partial huK}{\partial x} = \frac{1}{2} E_a u^3 + u_*^2 u - \varepsilon_0 h - \frac{1}{2} E_a u RCgh - \frac{1}{2} Rgh v_s (2C + E_s - c_b), \quad (33)$$

where  $u$  is the mean velocity,  $h$  the flow depth,  $K$  the mean turbulent kinetic energy,  $C$  the mean volume concentration (ratio of particle volume to total volume),  $E_a$  a coefficient of entrainment of surrounding fluid into the current,  $v_s$  the settlement velocity,  $E_s$  a coefficient of entrainment of particles from the bed into the current,  $c_b$  the near-bed particle concentration,  $R$  the specific submerged gravity of particles (ratio of buoyant density to ambient fluid density),  $u_*^2$  the bed shear velocity, and  $\varepsilon_0$  the depth-averaged mean rate of dissipation of turbulent energy due to viscosity. The main physical assumption in Parker *et al.*'s model is that the flow is considered as one-phase from a momentum point of view but treated as two-phase concerning the mass balance. Equation (30) states that the total volume variation results from entrainment of surrounding fluid. In (31), the variation in the mean solid concentration is due to the difference between the rate of particles entrained from the bed and the sedimentation rate. Equation (32) is the momentum balance equation: the momentum variation results from the driving action of gravity and the resisting action of bottom shear stress; depending on the flow depth profile, the pressure gradient can contribute either to accelerate or decelerate the flow. Equation (33) takes into account the turbulence expenditure for the particles to stay in suspension. Turbulent energy is supplied by the boundary layers (at the flow interfaces with the surrounding fluid and the bottom). Turbulent energy is lost by viscous dissipation ( $\varepsilon_0 h$  in (33)) as well as by mixing the flow (fourth and fifth terms in (33)) and maintaining the suspension against sedimentation flow mixing (last term on the right-hand side of (33)).

Although originally devoted to submarine turbidity currents, this model has been applied to airborne avalanches, with only small modifications in the entrainment functions (Fukushima & Parker, 1990; Gauer, 1995). A new generation of powder-snow avalanche models has recently appeared (Hutter, 1996). Some rely on the numerical resolution of local equations of motion, including a two-phase mixture approximation and closure equations, usually a  $k - \epsilon$  model for turbulence (Scheiwiller *et al.*, 1987; Sampl, 1993; Naaïm & Gurer, 1997). Other researchers have tried to establish the relation existing between a dense core and an airborne avalanche because they think that, most often, a powder-snow avalanche is tightly related to a denser part that supplies the airborne part with snow (Eglit, 1983; Nazarov, 1991; Issler, 1998). Though these recent

developments are undoubtedly a promising approach to modeling powder-snow avalanches, their level of sophistication contrasts with the crudeness of their basic assumptions as regards the momentum exchanges between phases, turbulence modification due to the dispersed phase, and so on. At this level of our knowledge of physical and natural processes, it is of great interest to continue to use simple models and to fully explore what they can describe and explain.

## 2.5 Three-dimensional computational models

The rapid increase in computer power has allowed researchers to integrate local motion equations directly. Compared to the depth-averaged models, the problems in the development of three-dimensional (3D) computational models mainly concern numerical treatments. For instance, the treatment of the free surface poses complicated issues. Naturally, problems linked to the constitutive equations reliable for snow are more pronounced compared to intermediate models since the entire constitutive equation must be known (not just the shear and normal stress). The development of 3D models is currently undertaken mainly for airborne avalanches generally using finite-volume codes for turbulent flows. Examples include the models by Naaïm & Gurer (1997), Hermann *et al.* (1993), and Scheiwiller *et al.* (1987).

## 2.6 Small-scale models

A few authors have exploited the similarities between avalanches and other gravity-driven flows. For instance, Hopfinger & Tochon-Danguy (1977) used the analogy between airborne avalanches and saline density currents to perform experiments in the laboratory in a water tank. In this way, examination of various aspects of airborne dynamics has been possible: effect of a dam, structure of the cloud, determination of the entrainment coefficients, etc. The chief issue raised by the analogy with density or gravity currents concerns the similarity conditions based on both the Froude (or equally the Richardson number) and Reynolds numbers (Hopfinger, 1983; Beghin & Olagne, 1991; Hopfinger & Tochon-Danguy, 1977). Regarding flowing avalanches, authors have considered the analogy with granular flows. Various materials (ping-pong ball, sand, beads) have been used. In engineering laboratory experiments simulating flowing avalanches offer promising tools for studying practical and complicated issues, such as the deflecting action of a dam (Chu *et al.*, 1995; Faug *et al.*, 2008) or braking mounds (Hákonardóttir *et al.*, 2003*a,b*).

## References

- ADJEL, G. 1996 Méthodes statistiques pour la détermination de la distance d'arrêt des avalanches. PhD thesis, Université Joseph Fourier.
- AMMAN, W., BUSER, O. & VOLLENWYDER, U. 1997 *Lawinen*. Birkhäuser.
- ANCEY, C. 1994 Modélisation des avalanches denses, approches théorique et numérique. *Houille Blanche* **5-6**, 25–39.
- ANCEY, C., ed. 1998 *Guide Neige et Avalanches : Connaissances, Pratiques, Sécurité*. Aix-en-Provence: Édisud.

- ANCEY, C. 2004 Powder-snow avalanches: approximation as non-Boussinesq clouds with a Richardson-number-dependent entrainment function. *J. Geophys. Res.* **109**, F01005.
- ANCEY, C. 2005 Monte Carlo calibration of avalanches described as Coulomb fluid flows. *Phil. Trans. Roy. Soc. London A* **363**, 1529–1550.
- ANCEY, C. 2006 *Dynamique des avalanches*. Lausanne: Presses Polytechniques et Universitaires Romandes.
- ANCEY, C. 2007 Plasticity and geophysical flows: A review. *J. Non-Newtonian Fluid Mech.* **142**, 4–35.
- ANCEY, C. & CHARLIER, C. 1996 Quelques réflexions autour d’une classification des avalanches. *Rev. Geog. Alpine* **84**, 9–21.
- ANCEY, C. & COCHARD, S. 2009 The dam-break problem for Herschel-Bulkley fluids down steep flumes. *J. Non-Newtonian Fluid Mech.* **158**, 18–35.
- ANCEY, C., COCHARD, S. & ANDREINI, N. 2009 The dam-break problem for viscous fluids in the high-capillary-number limit. *J. Fluid Mech.* **624**, 1–22.
- ANCEY, C., COCHARD, S., WIEDERSEINER, S. & RENTSCHLER, M. 2006 Front dynamics of supercritical non-Boussinesq gravity currents. *Water Resour. Res.* **42**, W08424.
- ANCEY, C., COCHARD, S., WIEDERSEINER, S. & RENTSCHLER, M. 2007 Existence and features of similarity solutions for supercritical non-Boussinesq gravity currents. *Physica D* **226**, 32–54.
- ANCEY, C., GERVASONI, C. & MEUNIER, M. 2004 Computing extreme avalanches. *Cold Regions Sci. Technol.* **39**, 161–180.
- ANCEY, C. & MEUNIER, M. 2004 Estimating bulk rheological properties of flowing snow avalanches from field data. *J. Geophys. Res.* **109**, F01004.
- ANCEY, C., MEUNIER, M. & RICHARD, D. 2003 The inverse problem for avalanche-dynamics models. *Water Resour. Res.* **39**, WR01099.
- BAINES, P.G. 2001 Mixing in flows down gentle slopes into stratified environments. *J. Fluid Mech.* **443**, 237–270.
- BEGHIN, P. 1979 Etude des bouffées bidimensionnelles de densité en écoulement sur pente avec application aux avalanches de neige poudreuse. PhD thesis, Institut National Polytechnique de Grenoble.
- BEGHIN, P. & BRUGNOT, G. 1983 Contribution of theoretical and experimental results to powder-snow avalanche dynamics. *Cold Regions Sci. Technol.* **8**, 63–73.
- BEGHIN, P., HOPFINGER, E.J. & BRITTER, R.E. 1981 Gravitational convection from instantaneous sources on inclined boundaries. *J. Fluid Mech.* **107**, 407–422.

- BEGHIN, P. & OLAGNE, X. 1991 Experimental and theoretical study of the dynamics of powder snow avalanches. *Cold Regions Sci. Technol.* **19**, 317–326.
- BERNARD, C.J.M.. 1927 Les avalanches. In *Cours de restauration des terrains de montagne*. Paris: École Nationale des Eaux et Forêts.
- BOUCHUT, F., MANGENEY-CASTELNAU, A., PERTHAME, B. & VILOTTE, J.-P. 2003 A new model of Saint Venant and Savage-Hutter type for gravity driven shallow flows. *C. R. Acad. Sci. Paris sér. I* **336**, 531–536.
- BOVIS, M.J. & MEARS, A.I. 1976 Statistical prediction of snow avalanche runout terrain variables in Colorado. *Artic Alpine Res.* **8**, 115–120.
- BOZHINSKIY, N. & LOSEV, K.S. 1998 The fundamentals of avalanche science. *Tech. Rep.* 55. EISFL.
- BRUGNOT, G. & POCHAT, R. 1981 Numerical simulation study of avalanches. *J. Glaciol.* **27**, 77–88.
- BUSER, O. & FRUTIGER, H. 1980 Observed maximum run-out distance of snow avalanches and determination of the friction coefficients  $\mu$  and  $\xi$ . *J. Glaciol.* **26**, 121–130.
- CHOW, V.T., ed. 1959 *Open-Channel Hydraulics*. New York: Mc Graw Hill.
- CHU, T., HILL, G., MCCCLUNG, D.M. & SHERKAT, R. 1995 Experiments on granular flows to predict avalanche runup. *Can. Geotech. J.* **32**, 285–295.
- COAZ, J.W. 1881 *Die Lawinen der Schweizer Alpen*. Bern: Schmid-Franke.
- COLBECK, S.C. 1991 The layer of snow cover. *Rev. Geophys.* **29**, 81–96.
- CONWAY, H. & C.F., RAYMOND 1993 Snow stability during rain. *J. Glaciol.* **39** (33), 635–642.
- CUI, X., GRAY, J.M.N.T. & JÓHANNESSON, T. 2007 Deflecting dams and the formation of oblique shocks in snow avalanches at Flateyri, Iceland. *J. Geophys. Res.* **122**, F04012.
- DENT, J.D. & LANG, T.E. 1980 Modelling of snow flow. *J. Glaciol.* **26**, 131–140.
- DENT, J.D. & LANG, T.E. 1982 Experiments on the mechanics of flowing snow. *Cold Regions Sci. Technol.* **5**, 243–248.
- DUFOUR, F., GRUBER, U. & AMMANN, W. 2001 Sur la piste des avalanches catastrophes. *Les Alpes* **2**, 9–15.
- ECKERT, N., PARENT, E., NAAIM, M. & RICHARD, D. 2008 Bayesian stochastic modelling for avalanche predetermination: from a general system framework to return period computations. *Stoch. Env. Res. Risk Ass.* **22**, 185–206.
- ECKERT, N., PARENT, E. & RICHARD, D. 2007 Revisiting statistical-topographical methods for avalanche predetermination: Bayesian modelling for runout distance predictive distribution. *Cold Regions Sci. Technol.* **49**, 88–107.

- EGLIT, E.M. 1983 Some mathematical models of snow avalanches. In *Advances in the Mechanics and the Flow of Granular Materials* (ed. M. Shahinpoor), pp. 577–588. Clausthal-Zellerfeld: Trans Tech Publications.
- EGLIT, M. 1998 Mathematical modeling of dense avalanches. In *25 Years of Snow Avalanche Research* (ed. Erik Hestnes), , vol. 203, pp. 15–18. Voss: Norwegian Geotechnical Institute.
- ELLISON, T.H. & TURNER, J.S. 1959 Turbulent entrainment in stratified flows. *J. Fluid Mech.* **6**, 423–448.
- FAUG, T., GAUER, P., LIED, K. & NAAIM, M. 2008 Overrun length of avalanches overtopping catching dams: Cross-comparison of small-scale laboratory experiments and observations from full-scale avalanches. *J. Geophys. Res.* **113**, F03009.
- FERNANDO, H.J.S. 1991 Turbulent mixing in stratified fluids. *Annu. Rev. Fluid Mech.* **23**, 455–493.
- FUKUSHIMA, Y., HAGIHARA, T. & SAKAMOTO, M. 2000 Dynamics of inclined suspension thermals. *Fluid Dyn. Res.* **26**, 337–354.
- FUKUSHIMA, Y. & PARKER, G. 1990 Numerical simulation of powder-snow avalanches. *J. Glaciol.* **36**, 229–237.
- GAUER, P. 1995 A model of powder snow avalanche. In *Les apports de la recherche scientifique à la sécurité neige, glace et avalanche* (ed. F. Sivardière), pp. 55–61. Chamonix: Cemagref.
- GRAY, J.M.N.T., TAI, Y.-C. & NOELLE, S. 2003 Shock waves, dead zones and particle-free regions in rapid granular free-surface flows. *J. Fluid Mech.* **491**, 161–181.
- GRAY, J.M.N.T., WIELAND, M. & HUTTER, K. 1998 Gravity-driven free surface flow of granular avalanches over complex basal topography. *Proc. R. Soc. London ser. A* **455**, 1841–1874.
- GRIGORIAN, S.S., EGLIT, M. E. & YAKIMOV, Y.L. 1967 A new formulation and solution of the problem of the motion of a snow avalanche (in Russian). *Trudy Vycokogornogo Geofizicheskogo Instituta* **12**, 104–113.
- HÁKONARDÓTTIR, K.M. & HOGG, A.J. 2005 Oblique shocks in rapid granular flows. *Phys. Fluids* **17**, 077101.
- HÁKONARDÓTTIR, K.M., HOGG, A.J., JÓHANNESSON, T., KERN, M.A. & TIEFENBACHER, F. 2003a Large-scale avalanche braking mound and catching dam experiments with snow: a study of the airborne jet. *Survey Geophys.* **24**, 543–554.
- HÁKONARDÓTTIR, K.M., HOGG, A.J., JÓHANNESSON, T. & TOMASSÓN, G.G. 2003b A laboratory study of the retarding effects of braking mounds on snow avalanches. *J. Glaciol.* **149**, 191–200.

- HARBITZ, K. 1999 A survey of computational models for snow avalanche motion. *Tech. Rep.*. Fourth European Framework Programme (ENV4-CT96-0258) Avalanche Mapping, Model Validation and Warning Systems.
- HERMANN, F., ISSLER, D. & KELLER, S. 1993 Numerical simulations of powder-snow avalanches and laboratory experiments in turbidity currents. In *International Workshop on Gravitational Mass Movements* (ed. L. Buisson & G. Brugnot), pp. 137–144. Grenoble: Cemagref.
- HOGG, A.J. & PRITCHARD, D. 2004 The effects of hydraulic resistance on dam-break and other shallow inertial flows. *J. Fluid Mech.* **501**, 179–212.
- HOGG, A.H. & WOODS, A.W. 2001 The transition from inertia- to bottom-drag-dominated motion of turbulent gravity current. *J. Fluid Mech.* **449**, 201–224.
- HOPFINGER, E.J. 1983 Snow avalanche motion and related phenomena. *Annu. Rev. Fluid Mech.* **15**, 45–76.
- HOPFINGER, E.J. & TOCHON-DANGUY, J.-C. 1977 A model study of powder-snow avalanches. *J. Glaciol.* **81**, 343–356.
- HUNT, B. 1994 Newtonian fluid mechanics treatment of debris flows and avalanches. *J. Hydraul. Eng.* **120**, 1350–1363.
- HUTTER, K. 1996 Avalanche dynamics. In *Hydrology of Disasters* (ed. V.P. Singh), pp. 317–392. Dordrecht: Kluwer Academic Publications.
- HUTTER, K., KOCH, T., PLÜSS, C. & SAVAGE, S.B. 1995 The dynamics of avalanches of granular materials from initiation to runout. Part II: Experiments. *Acta Mech.* **109**, 127–165.
- HUTTER, K., SIEGEL, M., SAVAGE, S.B. & NOHGUCHI, Y. 1993 Two-dimensional spreading of a granular avalanche down an inclined plane. Part I: Theory. *Acta Mech.* **100**, 37–68.
- ISSLER, D. 1998 Modelling of snow entrainment and deposition in powder-snow avalanches. *Ann. Glaciol.* **26**, 253–258.
- KERN, M.A., BARTELT, P., SOVILLA, B. & BUSER, O. 2009 Measured shear rates in large dry and wet snow avalanches. *J. Glaciol.* **55**, 327–338.
- KERN, M.A., TIEFENBACHER, F. & McELWAIN, J.N. 2004 The rheology of snow in large chute flows. *Cold Regions Sci. Technol.* **39**, 181–192.
- KEYLOCK, C.J. 2005 An alternative form for the statistical distribution of extreme avalanche runout distances. *Cold Regions Sci. Technol.* **42**, 185–193.
- KULIKOVSKIY, A.G. & SVEHNIKOVA, E.I. 1977 Model dlja rascheta dvizhija pilevoi snezhnoi lavini (a model for computing powdered snow avalanche motion) [in Russian]. *Materiali Glatsiologicheskikh Issledovanii [Data of Glaciological Studies]* **31**, 74–80.
- LA CHAPELLE, E.R. 1977 Snow avalanches: a review of current research and applications. *J. Glaciol.* **19**, 313–324.

- LACKINGER, B. 1986 Stability and fracture of the snow pack for glide avalanches. In *Avalanche formation, movement and effects* (ed. H. Gubler & B. Salm), pp. 229–241. Davos: IAHS, Wallingford, Oxfordshire, U.K.
- LAGOTALA, H. 1927 *Étude de l'avalanche des Pèlerins (Chamonix)*. Genève: Société Générale d'Imprimerie.
- LEVEQUE, R.J. 2002 *Finite Volume Methods for Hyperbolic Problems*. Cambridge: Cambridge University Press.
- LIED, K. & BAKKEHØI, S. 1980 Empirical calculations of snow avalanche run-out distances based on topographic parameters. *J. Glaciol.* **26**, 165–177.
- LIED, K. & TOPPE, R. 1989 Calculation of maximum snow avalanche runout distance based on topographic parameters identified by digital terrain models. *Ann. Glaciol.* **13**, 164–169.
- MAENO, O. 1993 Rheological characteristics of snow flows. In *International Workshop on Gravitational Mass Movements* (ed. L. Buisson & G. Brugnol), pp. 209–220. Grenoble: Cemagref.
- MCCLUNG, D.M. 2001 Extreme avalanche runout: a comparison of empirical models. *Can. Geotech. J.* **38**, 1254–1265.
- MCCLUNG, D.M. & LIED, K. 1987 Statistical and geometrical definition of snow avalanche runout. *Cold Regions Sci. Technol.* **13**, 107–119.
- MCCLUNG, D.M. & MEARS, A.I. 1991 Extreme value prediction of snow avalanche runout. *Cold Regions Sci. Technol.* **19**, 163–175.
- MCCLUNG, D.M. & SCHAEERER, P.A. 1993 *The Avalanche Handbook*. Seattle: The Mountaineers.
- MEUNIER, M. & ANCEY, C. 2004 Towards a conceptual approach to pre-determining long-return-period avalanche run-out distances. *J. Glaciol.* **50**, 268–278.
- MEUNIER, M., ANCEY, C. & TAILLANDIER, J.-M. 2004 Fitting avalanche-dynamics models with documented events from the Col du Lautaret site (France) using the conceptual approach. *Cold Regions Sci. Technol.* **39**, 55–66.
- MOUGIN, P. 1922 *Les avalanches en Savoie*, , vol. IV. Paris: Ministère de l'Agriculture, Direction Générale des Eaux et Forêts, Service des Grandes Forces Hydrauliques.
- NAAIM, M. & GURER, I. 1997 Two-phase numerical model of powder avalanche. Theory and application. *J. Natur. Hazards* **16**, 18.
- NAZAROV, A.N. 1991 Mathematical modelling of a snow-powder avalanche in the framework of the equations of two-layer shallow water. *Fluid Dynamics* **12**, 70–75.

- NOREM, H.F., IRGENS, F. & SCHIEDROP, B. 1986 A continuum model for calculating snow avalanche velocities. In *Avalanche formation, movement and effects* (ed. H. Gubler & B. Salm), pp. 363–379. Davos: IAHS, Wallingford, Oxfordshire, U.K.
- PARKER, G., FUKUSHIMA, Y. & PANTIN, H.M. 1986 Self-accelerating turbidity currents. *J. Fluid Mech.* **171**, 145–181.
- PERLA, R.I., CHENG, T.T. & MCCLUNG, D.M. 1980 A two-parameter model of snow-avalanche motion. *J. Glaciol.* **26**, 197–202.
- PUDASAINI, S.P. & HUTTER, K. 2006 *Avalanche Dynamics*. Berlin: Springer.
- DE QUERVAIN, R. 1981 *Avalanche Atlas*. Paris: Unesco.
- SALM, B., BURKARD, A. & GUBLER, H. 1990 Berechnung von Fließlawinen, eine Anleitung für Praktiker mit Beispielen. *Tech. Rep.* No 47. Eidgenössisches Institut für Schnee- und Lawinenforschung (Davos).
- SAMPL, P. 1993 Current status of the AVL avalanche simulation model – Numerical simulation of dry snow avalanches. In *International Workshop on Gravitational Mass Movements* (ed. L. Buisson & G. Brugnot), pp. 269–278. Grenoble: Cemagref.
- SAVAGE, S.B. 1989 Flow of granular materials. In *Theoretical and Applied Mechanics* (ed. P. Germain, J.-M. Piau & D. Caillerie), pp. 241–266. Amsterdam: Elsevier.
- SAVAGE, S.B. & HUTTER, K. 1989 The motion of a finite mass of granular material down a rough incline. *J. Fluid Mech.* **199**, 177–215.
- SAVAGE, S.B. & HUTTER, K. 1991 The dynamics of avalanches of granular materials from initiation to runout. Part I: Analysis. *Acta Mech.* **86**, 201–223.
- SCHEIWILLER, T., HUTTER, K. & HERMANN, F. 1987 Dynamics of powder snow avalanches. *Annales Geophysicae* **5B**, 569–588.
- SCHWEIZER, J., JAMIESON, J.B. & SCHNEEBELI, M. 2003 Snow avalanche formation. *Rev. Geophys.* **41**, 1016.
- STRAUB, D. & GRÊT-REGAMEY, A. 2006 A Bayesian probabilistic framework for avalanche modelling based on observations. *Cold Regions Sci. Technol.* **46**, 192–203.
- TAI, Y.-C., HUTTER, K. & GRAY, J.M.N.T. 2001 Dense granular avalanches: mathematical description and experimental validation. In *Geomorphological Fluid Mechanics* (ed. N.J. Balmforth & A. Provenzale), pp. 339–366. Berlin: Springer.
- TURNBULL, B., MCELWAIN, J. & ANCEY, C. 2007 The Kulikovskiy–Sveshnikova–Beghin model of powder snow avalanches: Development and application. *J. Geophys. Res.* **112**, F01004.

VILA, J.P. 1986 Sur la théorie et l'approximation numérique des problèmes hyperboliques non-linéaires, application aux équations de Saint-Venant et à la modélisation des avalanches denses. Ph. d. thesis, Paris VI.

VOELLMY, A. 1955 Über die Zerstörungskraft von Lawinen. *Schweizerische Bauzeitung* **73**, 159–162, 212–217, 246–249, 280–285.